# Afferent lymph-derived T cells and dendritic cells use different CCR7-dependent routes for lymph node entry and intranodal migration

Reinhold Forster, Asolina Braun, Tim Worbs, G. Leandros Moschovakis, Stephan Halle, Katharina Hoffmann, Jasmin Boelter, Anika Münk

# Afferent lymph-derived T cells and dendritic cells use different CCR7-dependent routes for lymph node entry and intranodal migration

Asolina Braun[1], Tim Worbs[1], G. Leandros Moschovakis[1], Stephan Halle[1], Katharina Hoffmann[1], Jasmin Bölter[1], Anika Münk[1] & Reinhold Förster[1]

[1]Institute of Immunology, Hannover Medical School, 30625 Hannover, Germany

Running title: LN homing via afferent lymphatics

×

Correspondence should be addressed to R.F. (foerster.reinhold@mh-hannover.de)

Prof. Dr. Reinhold Förster
Head and Director, Institute of Immunology
Hannover Medical School
D-30625 Hannover
GERMANY

fon: +49-511-532-9721
fax; +49-511-532-9722
email: foerster.reinhold@mh-hannover.de

Key words: homing, afferent lymphatics, dendritic cells, T cells, CCR7

Abbreviations used: **DCs** dendritic cell; **BM** bone marrow; **popLN** popliteal lymph node; **SCS** subcapsular sinus; **SHG** second harmonics generation; **WT** wild type; **TCZ** T cell zone; **MCoeff**, motility coefficient;

## Abstract

Little is known about the molecular mechanisms that determine lymph node (LN) entry and intranodal positioning of lymph-derived cells. By injecting cells directly into afferent lymph vessels of popliteal LNs, we demonstrate that lymph-derived T cells entered LN parenchyma primarily from peripheral medullary sinuses while dendritic cells (DCs) transmigrated through the floor of the afferent side subcapsular sinus. Transmigrating DCs induced local changes that allowed the concomitant entry of T cells at these sites. Signals mediated by the chemokine receptor CCR7 were absolutely required for the directional migration of both DCs and T cells into the T cell zone but dispensable for parenchymal entry of lymph-derived T cells and dendrite probing of DCs. These findings provide insights into molecular and structural requirements for LN entry and intranodal migration of lymph-derived immune cells.

## Introduction

During the last two decades, numerous molecules have been identified that regulate the homing of blood-derived lymphocytes to lymph nodes (LNs) via specialized high endothelial venules (HEVs). In contrast, surprisingly little is known about homing routes and mechanisms that control the LN entry of T cells and dendritic cells (DCs) that arrive with the afferent lymph. Within peripheral tissues, DCs constitutively sample the environment for antigen and eventually travel via afferent lymphatic vessels towards draining LNs designated here as primary LN. This process that has been shown to require chemotactic signals mediated by the chemokine receptor CCR7 (ref.[1,2]). Whereas the first migration step of Langerhans cells from epidermis to dermis is assumed to be CCR7-independent[2,3], epidermal as well as dermal DCs are subsequently guided towards small initial afferent lymphatics originating in the dermis by CCL21 expressed on the lymphatic endothelium[2,4]. Entry into these initial lymphatic vessels might occur predominantly via special preformed 'portals', independent of integrin-mediated adhesion and pericellular proteolysis[5-7]. Likewise, it has been suggested that entry of recirculating T cells into the initial lymphatic vessels also relies on CCR7 expression[8,9].

At least in murine LNs, the main producers for the CCR7-igands CCL19 and CCL21 are fibroblastic reticular cells of the T cell zone (TCZ) stromal compartment[10-12]. Additionally, HEV-bound CCR7-ligand contributes to the transmigration of lymphocytes through HEVs[10,13] whereas CCL21 present on stromal cells accelerates the basal velocity of randomly migrating T cells within the LN paracortex[14]. However, except for indirect indications from studies using *plt/plt* mice, a naturally occurring mutant lacking expression of the *Ccr7*-ligands CCL19 and CCL21 within secondary lymphoid organs[15], the influence of CCR7 and its ligands on lymph node entry and intranodal positioning of afferent lymph derived DCs and T cells remained unclear.

Naïve circulating T cells enter a LN via HEVs of blood vessels and leave the organ by accessing efferent lymphatics. From there, the cells may directly re-

enter blood circulation or immigrate into a LN located downstream (secondary LN) of the primary LN.

To systematically study the LN homing process of afferent lymph-derived DCs to primary as well as naïve T cells to secondary LNs, we established a new technique of intra lymphatic injection in mice that allowed the efficient delivery of arbitrary numbers of cells directly into the afferent lymph vessels of the popliteal LN (popLN). Combining this novel approach with two-photon microscopic imaging, we found that T cells, but not DCs, reached LNs downstream of the primary draining popLN after intra lymphatic injection. After transmigrating through the afferent side subcapsular sinus (SCS) floor of the popLN, wild-type DCs exhibited a highly directional migration towards the deep TCZ. In contrast, *Ccr7*-deficient (*Ccr7*$^{-/-}$) DCs exited the SCS with delayed kinetics and remained largely sessile within SCS-adjacent cortical regions while displaying comparable dendrite probing. On the other hand, T cells were not retained in the SCS in larger numbers following intra lymphatic delivery, but instead entered the LN parenchyma from peripheral medullary sinuses. Although wild-type as well as *Ccr7*$^{-/-}$ T cells displayed random walk motility within peripheral medullary cords, only wild-type T cells proceeded into the deep TCZ, probably by haptotaxis along an immobilized CCL21-gradient. Furthermore, mature DCs induced local changes of the SCS floor during transmigration that allowed the concomitant parenchymal entry of T cells at these sites.

## Results

### Distinct distribution of wild-type and *Ccr7*$^{-/-}$ DCs

We developed an experimental protocol that allows the micromanipulator-guided microinjection of immune cells directly into the afferent lymphatic vessel of the popLN in living mice ensuring the synchronized arrival of injected cells in the SCS. After intra lymphatic injection of ink, the dye was observed to almost immediately stain the efferent lymphatic vessel of the popLN, followed by the ipsilateral medial iliac LN (ilLN) and the renal LN (renLN) **(Supplementary Fig. 1a-c**). These findings not only confirm that also in mice lymphatic drainage occurs at least in part through LN chains but also imply that downstream LN receive efferent lymph containing naïve lymphocytes from more peripheral LN[16] (**Supplementary Fig. 1d**).

Next, we differentially labeled LPS-matured wild-type and *Ccr7*-deficient bone marrow-derived DCs (BMDCs; **Fig. 1a**) with the fluorescent cell tracers DDAO and TAMRA (and vice versa) before intra lymphatically injecting a 1:1 mixture. Two hours later, single cell suspensions of popLN, ilLN and renLN were prepared and analyzed by flow cytometry (**Fig. 1b**). While wild-type and *Ccr7*$^{-/-}$ BMDCs could be re-isolated at a ratio of 1:1 from primary draining popLN (**Fig. 1c**), we consistently failed to detect any BMDCs within ilLN or renLN (**Fig. 1d** and data not shown). These data indicate that afferent lymph-derived DCs are quantitatively retained within primary draining LN, and that this retention is independent of *Ccr7*. The subsequent intranodal fate of these DCs, was further investigated by intra lymphatic injections using 1:1 mixtures of TAMRA-labeled BMDCs together with BMDCs of mice expressing a ß-actin-eGFP transgene (eGFP BMDCs). As revealed by histology, wild-type BMDCs rapidly entered the parenchyma of the LN cortex by exiting mainly from SCS parts overlying interfollicular areas while sparing cortical B cell follicles. Starting to reach the outer paracortex within 2 h after intra lymphatic injection, wild-type BMDCs populated the entire TCZ 12 h and 24 h after delivery while concentrating in particular within deeper paracortical and medullary areas at 48 h (**Fig. 1d**). Of

interest, further histological analysis applying anti-LYVE-1 mAb on popLN sections collected 48 h after cell transfer indicates that few of the transferred DCs might actually enter the medullary sinuses and thus acquire the potential to disseminate to other organs (**Supplementary Fig 2**). In marked contrast, intra lymphatically injected *Ccr7*-deficient BMDCs entered the LN parenchyma with delayed kinetics and did not reach the paracortical TCZ throughout the observation period (**Fig. 1d**). A 3D reconstruction of a complete popLN collected 12 h after intra lymphatic DC transfer (**Fig. 1e** and **Supplementary Video 1**) further substantiates the massive intranodal migration and positioning defect of *Ccr7*-deficient DCs. Interestingly, early after intra lymphatic injection DCs were efficiently retained within the afferent hemisphere of the popLN, i.e. proximal to those sites where afferent lymph vessels merge with the SCS (**Fig. 1d**, **Supplementary Video 1**).

## LN entry and intranodal cellular dynamics of DCs

We next applied two-photon imaging to characterize the dynamic behavior of intra lymphatically applied DCs either *in vivo*[14] or *ex vivo* by superfusing the explanted popLN with oxygenated medium at 37°C in a custom-built imaging chamber[17]. We intra lymphatically co-injected TAMRA-labeled wild-type and eGFP-expressing *Ccr7*$^{-/-}$ BMDCs (and vice versa) at a ratio of 1:1, explanted the popLN 40 min later, and repeatedly imaged the same LN area over the next 8 h. Between 1 h and 4 h of cell transfer, wild-type DCs rapidly transmigrated through the floor of the afferent side SCS and exhibited a highly directional migration towards the central TCZ. Thus, at approximately 8 h after injection, most wild-type DCs had left the SCS as well as adjacent areas of the LN cortex. In remarkable contrast, most *Ccr7*-deficient BMDCs remained inside the SCS at 1 h. After 4 h and 8 h, only part of the *Ccr7*$^{-/-}$ cells had entered the LN parenchyma, generally residing in SCS-adjacent cortical areas (**Fig. 2a** and **Supplementary Video 2**). Some of the cells still residing in the SCS after 8 h might have undergone apoptosis since cell fragments were clearly visible at this point of time

(**Supplementary Video 2**). However, since this was more frequently observed with TAMRA-labeled than with eGFP-expressing DCs we assume that this effect is mainly caused by the cell labeling procedure. The intranodal migration behavior of wild-type eGFP BMDCs was characterized by extensive cell polarization resulting in the formation of a prominent leading edge as well as a pronounced long uropod, both features characteristic for directionally migrating cells (**Fig. 2b** and **Supplementary Videos 3,4**). While *Ccr7*$^{-/-}$ eGFP BMDCs also displayed dynamic changes of their cellular morphology, they hardly showed any prolonged directional cell polarization (**Fig. 2c** and **Supplementary Videos 3,4**) and consequently failed to translocate into the deeper LN paracortex. A more detailed view on migrating DCs confirmed these observations **(Fig. 2d,e).**

To specifically compare the intranodal probing behavior of wild-type and *Ccr7*$^{-/-}$ DCs, i.e. their ability to protrude and retract dendrites, we imaged eGFP-expressing BMDCs 6 h after transfer. The dendrite movement characteristics of these sedentary wild-type DCs were essentially indistinguishable from that of *Ccr7*-deficient DCs residing at similar locations within the LN cortex at 6 h (**Fig. 2f** and **Supplementary Video 5**). These findings strongly suggest that signals mediated via the chemokine receptor CCR7 are not required for efficient intranodal DC probing *in vivo*, which is in contrast to earlier *in vitro* observations suggesting that CCL19 contributes to the dendrite extension activity of DCs[18].

We then intra lymphatically injected DCs that had crawled out of split ear skin of CD11c-YFP mice. These cells also express high levels of CCR7 (**Supplementary Fig. 3a,b**). Two-photon microscopy revealed that skin-derived DCs as well entered the parenchyma of the popLN by transmigration through the floor of the SCS and exhibited cell polarization, uropod formation and inward directional migration comparable to that of eGFP-expressing wild-type BMDCs (**Fig. 2g** and **Supplementary Video 6**). Of note, skin-derived DCs characteristically displayed a more frequent branching of the leading edge during intranodal migration compared to wild-type BMDCs (**Supplementary Video 6**).

Quantitative migration analysis revealed that the average cellular velocity, straightness of migration, mean displacement plot as well as the motility

coefficient (MCoeff), were very similar between wild-type BMDCs and skin-derived CD11c-YFP DCs (**Fig. 2h**, black and green dots). Compared to their motility during *ex vivo* imaging, skin-derived CD11c-YFP DCs displayed slightly higher average cell velocities during intravital imaging, with essentially no difference in migration straightness, mean displacement or MCoeff (**Fig. 2h**, green and blue dots). Thus, the quantitative motility analysis confirmed our previous qualitative assessment that the migration behavior of wild-type BMDCs within explanted LN closely mirrored the physiological situation. Importantly, in comparison to all wild-type DC groups analyzed, *Ccr7*-deficient BMDCs exhibited reduced average cell velocities, migration straightness and mean displacement over time, resulting in a ~4-fold reduced MCoeff (**Fig. 2h**; gray dots).

### *Ccr7*$^{-/-}$ DCs are potent inducers of LN shutdown

During the so-called 'LN shutdown' reaction, the homing of inflammatory DCs is thought to induce the intranodal accumulation of lymphocytes resulting in LN swelling. 72 h after intra lymphatic injection of 5,000 wild-type or *Ccr7*$^{-/-}$ BMDCs we observed a comparable increase in lymphocyte numbers irrespective of the DC genotype (**Fig. 3a**). It is well established that following subcutaneous injection of DCs only a small fraction of wild-type DCs actually enters the afferent lymphatic vessels and subsequently the connecting LN[19]. Therefore, we used substantially higher numbers of DCs ($1\times10^5$) for subcutaneous application into the hind footpad. While the injection of wild-type BMDCs via this route led to a ~11-fold increase in cell count of the draining popLN, the application of the same number of *Ccr7*-deficient DCs only resulted in a ~4-fold increase (**Fig. 3a**). Thus, the efficiency of LN homing, i.e. arrival in the SCS of the draining LN, contributes to the degree of LN shutdown induced by migratory DCs, while the intranodal positioning has no major influence on this process, substantiating former findings[20,21] that locally produced soluble mediators rather than direct cell-cell interactions transiently inhibit lymphocyte egress.

## Reduced T cell proliferation *in vivo* by *Ccr7*$^{-/-}$ DCs

We next employed TCR transgenic OT-I T cells specific for the ovalbumin-derived SIINFEKL peptide as reporter cells to test whether misplaced DCs are impaired in activating T cells. CFSE-labeled OT-I T cells were adoptively transferred by intravenous injection into bm1 recipient mice, which are unable to cross-present the SIINFEKL peptide. Subsequently, DCs were delivered intra lymphatically and T cell proliferation was analyzed 65 h later. In comparison to their wild-type counterparts, *Ccr7*-deficient DCs were less efficient in inducing the antigen-specific proliferation of naïve T cells (**Fig. 3b,c**), indicating that the CCR7-dependent inward migration of DCs into the paracortex indeed contributes to T cell activation efficiency.

### LN entry of T cells via afferent lymphatics

LNs are often organized in chains, implying that lymphocytes exiting a peripheral primary LN via efferent lymphatics will arrive in the SCS of a more central secondary LN via an afferent lymph vessel **(Supplementary Fig. 1).** To study the homing of lymph-derived T cells, we intra lymphatically co-injected $2\times10^4$ TAMRA-labeled CD4$^+$ wild-type T cells and $2\times10^4$ eGFP-expressing *Ccr7*$^{-/-}$ CD4$^+$ T cells (and vice versa). In contrast to the situation observed for DCs, wild-type as well as *Ccr7*$^{-/-}$ T cells localized predominantly to outer parts of the peripheral medullary sinus system, which includes the capsule-lining sinus of the medullary LN hemisphere (**Fig. 4a**; see also (**Supplementary Fig. 4**) for topological details). Furthermore, while DCs were found to home exclusively into the primary draining popLN, considerable numbers of T cells were present in the downstream 2$^{nd}$ level ilLN at 2 h and 24 h after intra lymphatic injection (**Supplementary Fig. 5**). Two hours after intra lymphatic application, some wild-type T cells had already reached the outer paracortex of the primary draining popLN, while at 4 h wild-type T cells were found to populate the entire TCZ. In contrast, most intra lymphatically injected *Ccr7*$^{-/-}$ T cells remained within outer peripheral medullary areas at all time points analyzed (**Fig. 4a**).

LN entry routes were further analyzed using anti-LYVE-1-mAb to delineate the peripheral medullary sinus system from the parenchymal compartment of the peripheral medullary cords (**Fig. 4b**; see also **Supplementary Fig. 4** for orientation). *Ccr7*-deficient T cells were able to leave the lumen of the peripheral medullary sinus system, thus efficiently entering the LN parenchymal compartment. Four hours after intra lymphatic injection *Ccr7*$^{-/-}$ T cells displayed a pronounced accumulation within peripheral medullary cords which are characterized by a more densely packed cellular environment as revealed by nuclear DAPI staining (**Fig. 4b**). Since we found T cells to initially concentrate within the peripheral medullary sinus system following intra lymphatic delivery, we checked whether passive transport and deposition due to the fluid dynamics of lymph flow could result in such a preferential accumulation of lymphocytes. To this end, we used the intra lymphatic injection setup to apply fluorescent 6 µm latex microspheres as inert model particles. Of interest, also these particles primarily deposited within outer parts of the peripheral medullary sinus system (**Fig. 4c**).

The distribution of lymph fluid and lymph-borne T cells within the LN sinus system was further analyzed by intra lymphatically injecting TAMRA-labeled *Ccr7*$^{-/-}$ CD4$^{+}$ T cells, followed by the application of a soluble fluorescent tracer (fixable FITC-conjugated high molecular weight dextran) via the same route 15 min later. Another 5 min later, the recipient mice were sacrificed and the draining popLN analyzed by histology. Intra lymphatically injected *Ccr7*-deficient T cells were found to reside mainly in superficial parts of the peripheral medullary sinus system lumen that had also been reached by the soluble fluorescent tracer (**Fig. 4d**). Taken together, these observations suggest that, to a large extent, afferent lymph-derived T cells are passively transported by lymph flow into the peripheral medullary sinus system. Subsequently, they can cross the LYVE-1$^{+}$ endothelium and thereby enter the LN parenchyma independently of CCR7 signals by migrating into adjacent peripheral medullary cords.

**Migration dynamics of afferent lymph-derived T cells**

We next aimed to delineate the boundaries between medullary sinuses and cords during two-photon microscopy by visualizing the LYVE-1-positive lymphatic endothelium *in vivo*. To this end, labeled anti-Lyve1-mAb was intra lymphatically applied 30 min before delivering eGFP-expressing $CD4^+$ wild-type T cells via the same route. Numerous wild-type T cells were found to enter peripheral medullary cords by directly transmigrating through the floor of the capsule-lining medullary sinus (**Fig. 5a,b** and **Supplementary Video 7**). Interestingly, in some cases several wild-type T cells were found to cross the LYVE-$1^+$ lymphatic endothelial layer of the sinus floor at the same place within a short period of time (**Supplementary Video 7**). These "hot spots" might represent pre-formed or temporarily induced "transmigration portals" within the capsule-lining medullary sinus floor. Alternatively, intra lymphatically injected wild-type T cells can enter the LN parenchyma by transmigrating through the LYVE-$1^+$ boundary of inner peripheral medullary sinus system branches after migration within the sinus lumen (**Fig. 5c** and **Supplementary Video 8**).

To comprehensively visualize the 3D topology of LYVE-$1^+$ sinus boundaries, we used the software Imaris to generate 3D isosurface models that allowed us to clearly differentiate between sinus lumen and LN parenchyma (**Fig. 5d** and **Supplementary Video 9**). The compartmental distribution and intranodal migration behavior of wild-type T cells during the first 0.5-2 h following intra lymphatic delivery, was analyzed by semi-automated tracking of T cells that had already left the capsule-lining medullary sinus at the beginning of track analysis. To determine their subsequent distribution between peripheral medullary cords and peripheral medullary sinus system, a 'dwell index' was calculated as the ratio (parenchyma vs. sinus lumen) of the accumulated dwell times (i.e. track durations) of all wild-type T cells tracked within each compartment. The obtained dwell index (P/S) of ~2.2 (**Fig. 5e**) indicates that early after intra lymphatic injection, wild-type T cells had a more than 2-fold preference to migrate within peripheral medullary cords, i.e. within LN parenchyma. Once located within a compartment, wild-type T cells largely respected compartmental boundaries during migration in the peripheral medulla, as ~75% of all cell tracks did not cross

the LYVE-1$^+$ endothelium of peripheral medullary sinuses. Most of those cell that transmigrated did so only once, and no T cell was observed to transmigrate more than three times during the imaging period of 40-60 min (**Fig. 5f**). Finally, when classifying all cell tracks according to the compartment in which the cell resided at the end of the imaging period (**Fig. 5g**), a preferential migration of wild-type T cells into and within peripheral medullary cords became obvious: While more than 70% of all cell tracks were localized completely within peripheral medullary cords, less than 5% of the T cells stayed within the lumen of peripheral medullary sinuses throughout the imaging. Regarding the ~25% of wild-type T cells which had changed the compartment (at least once), 4 times more (~20% vs. ~5%) T cells were located in the peripheral medullary cords at the end of imaging. In summary, T cells preferentially migrated in peripheral medullary cords rather than returning into the peripheral medullary sinus system early after arrival via afferent lymphatics.

The rapid and preferential localization into the parenchymal compartment after intra lymphatic application was also observed for *Ccr7*$^{-/-}$ CD4$^+$ T cells during two-photon imaging (**Supplementary Video 10**). However, while wild-type T cells exhibited a pronounced inward migration towards the paracortex displaying high directionality and displacement over time, most *Ccr7*-deficient T cells exhibited an apparent random walk migration that was largely restricted to peripheral medullary cords (**Fig. 6a** and **Supplementary Video 10**). Although the average migration speed of *Ccr7*$^{-/-}$ CD4$^+$ T cells was only slightly lower (**Fig. 6b**), their movement was much more confined compared to their wild-type counterparts as evidenced by decreased motility parameters of directionality (track straightness, **Fig. 6b**) and displacement over time (mean displacement plot and MCoeff, **Fig. 6b**).

Hypothesizing that afferent lymph-derived T cells might utilize CCR7-derived signals as guidance cues in order to successfully navigate from peripheral medullary cords to the paracortical TCZ, we analyzed the distribution of the

CCR7-ligand CCL21 within peripheral medullary areas by immunohistology and found increased CCL21 expression towards the LN center (**Fig. 6c**).

**Altered T cell homing in the presence of mature DCs**

When applied alone, afferent lymph-derived T cells entered the LN parenchymal compartment from the peripheral medullary sinus system lumen while intra lymphatically injected DCs were observed to directly transmigrate through the floor of the afferent side SCS. This raised the question whether, apart from flow dynamics, morphological properties of the SCS floor might prevent the transmigration of T cells at this site under steady state conditions. As revealed by two-photon imaging of the afferent side SCS 30 min after intra lymphatic application, $CD4^+$ wild-type T cells remained almost completely restricted to the SCS lumen, exhibiting only very limited motility (**Fig. 7a**, **Supplementary Video 11**). In stark contrast, once wild-type BMDCs were intra lymphatically applied 40 min earlier, afferent lymph-derived wild-type T cells transmigrated through the SCS floor and displayed an avid inward migration at sites of DC transmigration (**Fig. 7b**, **Supplementary Video 11**). To test for a potential role of LPS protracted probably in trace amounts into the SCS by *in vitro* matured DCs we also intra lymphatically delivered T cells that had been incubated with the same concentrations of LPS used for DC maturation. Since under these experimental conditions T cells were still excluded to efficiently home via the SCS **(Supplementary Video 12)** our findings suggest, that DCs play an important role in the induced homing of T cells via this route.

Hypothesizing that an altered penetrability might correlate with morphological changes of the SCS floor, we applied immunohistology to analyze in greater detail the configuration of the sinus-parenchyma border within different LN regions. After intra lymphatic injection of inert fluorescent microspheres or $CD4^+$ wild-type T cells alone, the cellular composition and morphology of the SCS remained virtually unchanged compared to steady-state conditions (**Fig. 7c,d** and data not shown): The SCS floor of the afferent popLN hemisphere was composed of a thin layer of LYVE-$1^+$ lymphatic endothelial cells as well as

numerous CD169$^+$ SCS-lining macrophages that displayed an outspread cellular morphology, extending into the SCS lumen (**Fig. 7c,d**). In contrast, medullary sinuses were characterized by a much stronger endothelial LYVE-1 expression with only few solitary CD169$^+$ macrophages lining the parenchymal surface of these sinus structures. Instead, CD169$^+$ macrophages were interspersed within the lumen of medullary sinuses, in particular concentrating towards the central hilar region of the medulla (**Fig. 7c-e** and **Supplementary Fig 4**). Strikingly, the transmigration of intra lymphatically injected wild-type BMDCs was found to induce profound morphological changes of the afferent side SCS floor (**Fig. 7e**): SCS-lining CD169$^+$ macrophages appeared elongated and aligned in parallel to immigrating DCs, while the LYVE-1-signal within the SCS floor was largely diminished. These effects were clearly restricted to parts of the SCS, which harbored high numbers of immigrating DCs.

## Discussion

Little is known about mechanisms regulating LN entry of cells that arrive via afferent lymphatics. This is in primarily due to the generally low frequency of subcutaneously injected cells that actually enter afferent lymphatic vessels and thus reach the draining LN. To overcome this fundamental limitation, we established a new micro-injection technique in mice to deliver defined immune cell populations directly into the afferent lymph vessel of the popLN. Although we consider intra lymphatic injection as a major technical advance, it should be mentioned that this procedure not necessarily reflects the naturally occurring scenario of cells which are unlikely to arrive as a bolus via afferent lymphatics during steady state or inflammatory conditions. Using intra lymphatic cell infusion we found four fundamental differences in the LN homing behavior of afferent lymph-derived DCs and T cells: (1) Initial positioning after intra lymphatic application (2) location and degree of CCR7-dependency of parenchymal entry (3) route and character of intranodal migration and (4) degree of confinement to the primary draining LN.

Directly after intra lymphatic injection, T cells accumulated within the peripheral medullary sinus system where the capsule-lining medullary sinus (as a direct extension of the afferent side SCS) connects to the first branches of peripheral medullary sinuses. The labyrinthine branching of the peripheral medullary sinus system probably causes a relatively abrupt reduction of the fluid velocity of lymph flow, which in turn might result in the observed preferential deposition of lymphocytes and latex beads within the peripheral medullary sinus system. In contrast, intra lymphatically injected DCs were found almost exclusively within the SCS lumen of the afferent LN hemisphere. This might be either a consequence of differences in cell size and shape, leading to a faster passive deposition of the larger DCs and – or, result from active retention of DCs.

Importantly, the initial distribution of DCs within the SCS not only influences the site of parenchymal entry but probably contributes to the strict confinement of

afferent lymph-derived DCs homing to the primary draining LN as well. This in turn might favor the regional compartmentalization or alternatively, the functional specialization of adaptive immune responses that are elicited by migratory DCs, or represent a general protective mechanism to prevent the systemic spread of cell-bound antigen (e.g. early during a local infection). In this context, it is noteworthy that the presentation of cell-bound but not soluble antigen has been shown to efficiently induce mechanisms of peripheral tolerance[22].

Interestingly, wild-type and *Ccr7*$^{-/-}$ T cells entered the LN parenchymal compartment with comparable efficiency while the exit of afferent lymph-derived DCs from the SCS was severely impaired in the absence of CCR7 signals. This probably reflects, at least in part, the high intrinsic motility of T lymphocytes that supports a basic random walk migration even in the absence of functional CCR7-interactions[14]. DCs, in contrast, seem to rely heavily on chemotactic or haptotactic CCR7 cues[23] in order to achieve cell polarization, cytoskeletal reorganization, and consequently directional migration into the LN parenchyma.

Once inside the LN parenchyma, both DCs and T cells strictly required CCR7-signals in order to translocate into the deeper paracortical TCZ, but displayed different characteristics during intranodal migration: While DCs followed straight pathways through interfollicular cortical regions, indicative for a strong chemotactic or haptotactic guidance as described by Schumann et al.[23], T cells seemed to progress from peripheral medullary cords into the TCZ by means of a ‘skewed’ random walk: As it has been proposed for naïve T cells migrating within the paracortical TCZ after entry via HEV[24,25], afferent lymph-derived T cells might utilize the stromal cell network as a scaffold for basic random walk migration. Increasing concentrations of immobilized CCL21 might then bias the migration of wild-type T cells towards the LN center, resulting in the observed ‘skewed’ random walk into the TCZ.

Upon arrival via afferent lymph, wild-type as well as *Ccr7*$^{-/-}$ T cells largely respected compartmental boundaries while navigating within the complex topology of peripheral medullary areas and preferentially migrated within peripheral medullary cords. This might reflect a certain structural barrier function

of the LYVE-1$^+$ endothelial cell layer making up the wall of medullary sinuses or, more likely, result from a preferential 'adherence' of migrating T cells to the surface of parenchymal stroma cells.

Importantly, medullary sinuses are directly connected to the efferent lymph vessel and have been regarded, in addition to recently described cortical sinuses[26-28], as important 'exit structures' for the LN egress of lymphocytes. So the question arises how medullary sinuses can, at the same time, serve for both lymphocyte homing and egress. Fundamental work by the group of Cyster and others identified the sphingosine-1-phosphate receptor 1 ($S1P_1$) as the most important egress-promoting receptor on T lymphocytes (reviewed in[29,30]). While being largely absent in LN parenchyma, sphingosine-1-phosphate, a ligand for $S1P_1$, has been shown to be present at high concentrations in lymph fluid. This gradient guides lymphocytes from LN parenchyma into medullary and cortical sinuses, thus facilitating their egress. Of interest, lymphocytes within lymph lack surface $S1P_1$ (ref.[31]) and ligand binding has been shown to induce a transient internalization of the receptor, thus rendering cells unresponsive to S1P[32]. Together, these data suggest a scenario in which lymph-derived wild-type as well as *Ccr7*-deficient T cells would be temporarily unresponsive to a sinus lumen-retaining S1P signal, thus efficiently entering peripheral medullary cords. On the other hand, CCR7-ligands expressed on stromal cells within LN parenchyma have been shown to provide a functional counterpart that helps to retain T cells within this compartment[26]. Wild-type but not *Ccr7*$^{-/-}$ T cells could then follow an immobilized CCL21 gradient to progress into the paracortical TCZ. Due to low intranodal S1P-concentrations, afferent lymph-derived T cells should regain their $S1P_1$-surface expression with increasing LN dwell time, similar to T cells that have homed via HEV. Consequently, medullary sinuses most probably also function as exit sites for lymph-derived T cells at later time points.

Our preliminary analysis regarding the homing efficiency of lymph-derived naïve wild-type T cells revealed that 2 h after intra lymphatic delivery, approximately 15% of the total injected T cells were present in the popLN, and 5% in the respective 2$^{nd}$ level ilLN (data not shown). These observations suggest that

homing via afferent lymphatics can considerably contribute to LN homing of naïve T cells, probably most relevant in the case of downstream LN receiving afferent lymph-derived naïve T cells that have previously egressed from a more peripheral LN.

Furthermore, mature DCs actively transmigrating through the SCS induce changes in the SCS floor morphology that additionally allow the direct entry of afferent lymph-derived T cells. This might represent a strategy to increase not only the LN homing frequency of lymph-derived T cells but also the likelihood of DC-T cell interactions within interfollicular areas, potentially facilitating the reactivation of tissue-derived memory T cells as well as the priming of naïve T cells under conditions of acute inflammation.

The relatively efficient T cell proliferation induced by *Ccr7*-deficient DCs in these LN regions further supports this idea. These results also emphasize the obvious potential of naïve T lymphocytes to scan large volumes of LN parenchyma and indicate that, in addition to the paracortical TCZ, interfollicular cortical areas can provide a suitable environment for productive T cell-DC encounters as suggested before[33]. Since different subpopulations of migratory DCs have been described to pass through and accumulate within distinct subcompartments of the LN[33,34], it seems possible that functionally specialized T cell immune responses could be primed at different intranodal locations.

Representing an efficient approach for the targeting of defined cell populations to peripheral LN, the intralymphatic injection technique described here will allow to further elucidate numerous aspects of LN development, function and homeostasis. Furthermore, it might also help to unravel the series of events occurring during LN invasion and spread of tumors metastasizing via lymphatics.

## Acknowledgments

This work was funded by DFG grants SFB566-A14, SFB587-B3 and EXC62, “Rebirth” to RF. AB is a scholarship holder of the Boehringer Ingelheim Fonds. We thank M. Herberg for excellent animal care, E. Kremmer (Helmholtz Zentrum München, Germany) for providing antibodies, and G. Bernhardt for discussion and critical comments on the manuscript.

## Competing financial interests

The authors declare no conflicting financial interests.

## Author contributions

R.F., A.B. and T.W. designed experiments, analyzed data and wrote the paper; A.B. performed experiments, including intralymphatic. injections; T.W. contributed to Fig. 1, two-photon imaging and data analysis; S.H. contributed to Fig. 7, read and commented on manuscript; G.L.M. contributed to Supplementary Fig. 2, read and commented on manuscript; A.M., K.H., J.B. performed histology, FACS stainings and DC cell cultures.

# Legends to Figures

**Figure 1. *Ccr7*$^{-/-}$ BMDCs do not reach the paracortical TCZ after intralymphatic application.** (**a**) Comparable expression of CD11c and MHCII by DCs generated *in vitro* from BM of WT and *Ccr7*$^{-/-}$ donors. (**b**) WT and *Ccr7*$^{-/-}$ BMDCs were differentially labeled with DDAO or TAMRA (and vice versa) and mixed at a ratio of 1:1. 2 h after intra lymphatic injection of $2.5\times10^5$ total cells, popLN DCs were isolated by enzymatic digestion and analyzed by flow cytometry. (**c**) Ratio of WT to *Ccr7*$^{-/-}$ BMDCs retrieved from the draining popLN as described above. Mean+SD is shown. n=11 LN, 3 independent experiments. (**d**) $1x10^5$ cells of a 1:1 mixture of eGFP-expressing WT and TAMRA-labeled *Ccr7*$^{-/-}$ BMDCs were injected intra lymphatically in 5 µl PBS, and popLN and iLN were harvested at the time points indicated. Experiments have been repeated using eGFP-expressing *Ccr7*$^{-/-}$ and TAMRA-labeled WT BMDCs yielding comparable results (not shown). Scale bars, 100 µm. n=4-12 LN per time point, 2-5 independent experiments; M, orientation of the central medulla-hilus region. (**e**). To visualize the divergent positioning of intra lymphatically injected WT and *Ccr7*$^{-/-}$ BMDCS, a popLN explanted 12 h after cell transfer (see **Fig. 1d**) was sectioned completely and the composite images acquired by fluorescence microscopy were assembled in Fiji to generate a 3D-reconstruction (see **Supplementary Video 1**); scale bar, 200 µm. (**f**) iLN from mice shown in **d** were collected and analyzed for the presence of intra lymphatically injected BMDCs; scale bar, 100 µm.

**Figure 2. Intranodal migration behavior of intra lymphatically injected DCs as visualized by two-photon microscopy.** (**a**) 40 min after intra lymphatic injection of $3\times10^3$ TAMRA-labeled WT (red) and $3\times10^3$ eGFP-expressing *Ccr7*$^{-/-}$ (green) BMDCs, the draining popLN was explanted and the same LN area imaged *ex vivo* at 1 h, ~4 h and ~8 h after cell transfer to demonstrate long-term development of intranodal DC positioning. WT but not *Ccr7*$^{-/-}$ BMDCs exhibit a pronounced inward directional migration (see also **Supplementary Video 2**).

Second harmonics generation signal (SHG) of collagen fibers of the LN capsule is shown in blue, n=7-19 LN and ≥4 independent experiments per time point for **a-e**. (**b**) WT BMDCs show directional migration and distinct uropod formation during the first ~4 h after arrival in the SCS. Start of *ex vivo* time lapse (0 min, left panel) is 3 h after intra lymphatic injection of $2\times10^3$ eGFP-expressing WT BMDCs (green), time scale of DCs tracks (right panel) is color-coded. (**c**) *Ccr7*$^{-/-}$ BMDCs largely remain within or near the SCS and do not form uropods. Start of *ex vivo* time lapse (0 min, left panel) is 4 h 20 min after intra lymphatic injection of $2.5\times10^3$ eGFP-expressing *Ccr7*$^{-/-}$ BMDCs (green), time scale of DCs tracks (right panel) is color-coded. The time lapse recordings of **b** and **c** are shown in **Supplementary Video 3**, note that several *Ccr7*$^{-/-}$ BMDCs migrated outwards towards the SCS in the course of imaging; scale bars, 50 µm for **a**-**c**. (**d,e**) Cellular morphology of eGFP-expressing BMDCs (green) during intranodal migration. SHG signal (blue) at the top indicates position of SCS. (**d**), During early directional migration, WT BMDCs are highly polarized, displaying a pronounced leading edge and uropod. Start of *ex vivo* time lapse (0min, left panel) is 1.5 h after intra lymphatic injection of $2x10^3$ WT BMDCs. (**e**), *Ccr7*$^{-/-}$ BMDCs do not show any pronounced cell polarization and reach the SCS-adjacent LN parenchyma only at later time points. Start of *ex vivo* time lapse (0 min, left panel) is 3 h 45 min after intra lymphatic injection of $2.5\times10^3$ *Ccr7*$^{-/-}$ BMDCs. The time lapse recordings of **d** and **e** are shown in **Supplementary Video 4**; scale bars in **d** and **e**, 10 µm. (**f**) WT and *Ccr7*$^{-/-}$ BMDCs exhibit comparable dendrite movement and probing behavior. Dendrite morphology was analyzed after the directional migration of WT BMDCs had ceased. Start of *ex vivo* time lapse (0 min, leftmost panel) is 6 h 30 min after intra lymphatic injection for WT and 6 h for *Ccr7*$^{-/-}$ BMDCs, respectively (see also **Supplementary Video 5**); scale bar, 5 µm. 1.5-$3.5\times10^3$ injected cells, n=6-8 LN from 6 independent experiments (**g**) After intra lymphatic application, primary skin-derived WT DCs exhibit an intranodal migration comparable to WT BMDCs (as shown in **b**). Start of *ex vivo* time lapse (0 min, left panel) is 2 h after intra lymphatic injection of $3.5\times10^3$ skin-emigrated CD11c-YFP WT DCs (green), time scale of DC tracks

(right panel) is color-coded (see also **Supplementary Video 6**). SHG signal of collagen fibers of the LN capsule is shown in blue; n=6 LN, 3 independent experiments; scale bar 50 µm (**h**) Statistical analysis of the intranodal DC migration behavior. For average track speed and track straightness, dots represent individual cell tracks, bars indicate median values. For motility coefficient (MCoeff), dots represent single time lapse recordings of different imaging days, bars indicate mean values. Mean displacement plots are calculated using one representative time lapse recording per group.

**Figure 3. Intranodal positioning of afferent lymph-derived DCs contributes to T cell proliferation but not LN shutdown** (**a**) In order to compare the degree of LN shutdown induction, WT (black bars) or *Ccr7*$^{-/-}$ (white bars) BMDCs (or PBS as control, Ctrl., grey bars) were injected intra lymphatically ($5\times10^3$ cells per afferent lymph vessel) or subcutaneously ($1\times10^5$ cells per footpad). 72h later, total living cell numbers of the draining popLN were determined by cell counting. **P*<0.01; ***P*<0.001; n.s., not significant; unpaired two-tailed Student's *t* test; mean+SD, n=8-15 mice from 3-4 independent experiments (**b**, **c**) T cell proliferation induced by antigen-loaded *Ccr7*$^{-/-}$ BMDCs applied intra lymphatically is reduced in comparison to WT controls. At day -1, $1.5\times10^7$ CFSE-labeled OTI Ly5.1 cells were adoptively transferred by i.v. injection into bm1 recipients. At day 0, $5\times10^3$ SIINFEKL-peptide-pulsed WT (black dots) or *Ccr7*$^{-/-}$ (white dots) BMDCs (or PBS as control, grey dots) were injected intra lymphatically into the same animals and 65 h later, T cell proliferation was analyzed by FACS. (**b**) Representative CFSE profiles of $CD8^+$, Ly $5.1^+$, $V\alpha2^+$, $V\ß5^+$ lymphocytes isolated from the draining popLN (black line) after intra lymphatic injection of antigen-loaded WT (upper panel) or *Ccr7*$^{-/-}$ (lower panel) BMDCs. CFSE profiles of brachial LN of the same animals (shaded area) are shown as control. (**c**) The proliferation index was calculated using the automated proliferation function of FlowJo, cell cycle number was adjusted to obtain an equation with the smallest root mean square. Each dot represents an individual popLN, bars indicate mean

values, n=12 per group from three independent experiments; **$P$<0.001 (unpaired two-tailed Student's $t$ test).

**Figure 4. After intralymphatic injection, CD4 T cells enter LN parenchyma primarily within peripheral medullary areas and require CCR7-signals for migration into the paracortical TCZ.** (**a**, **b**) Immunohistological analysis of draining popLN after intra lymphatic injection of $2\times10^4$ TAMRA-labeled WT (red) and $2\times10^4$ eGFP-expressing *Ccr7*$^{-/-}$ (green) polyclonal CD4$^+$ T cells (and vice versa, not shown). n=15 per time point from 5 independent experiments (**a**) Overview composite images illustrating the differential intranodal positioning of $2\times10^4$ each, WT (red) and *Ccr7*$^{-/-}$ (green) CD4 T cells 2 h (upper panel) and 4 h (lower panel) after intra lymphatic injection. IgD staining (blue) marks B cell follicles as well as medullary B cells. M, orientation of the central medulla-hilus region; scale bars, 100 µm. (**b**) *Ccr7*$^{-/-}$ CD4 T cells (green) accumulate within peripheral medullary cords (white arrowheads) at 4h but do not proceed into the deep paracortex. LYVE-1 staining (blue) of lymphatic endothelium highlights sinus structures. The peripheral medullary sinus lumen (white arrow) is less densely packed with cells as illustrated by DAPI nucleus staining (white, upper panel); scale bars, 20 µm. (**c**) Comparable to CD4 T cells, inert 6 µm latex beads (green) are concentrated within the lumen of LYVE-1$^+$ peripheral medullay sinus structures (red) 15 min after intra lymphatic application of $2\times10^4$ beads. n=6 from 2 independent experiments (**d**) Fluid flow seems to determine the initial deposition of T cells predominantly within peripheral medullary sinuses directly after intra lymphatic injection. 15 min after intra lymphatic application of $2\times10^4$ TAMRA-labeled *Ccr7*$^{-/-}$ CD4 T cells (red), 5 µL fixable FITC-conjugated 500 kDa Dextran (green) was injected into the same afferent lymph vessel and further 5 min later draining popLN were isolated and fixed with paraformaldehyde. LYVE-1 staining (blue) of lymphatic endothelium highlights sinus structures; n=12 from 2 independent experiments; scale bars, 50 µm for **c**, **d**.

**Figure 5. Two-photon imaging of LN entry events of intra lymphatically injected CD4 T cells within peripheral medullary areas.** (**a, b**) Examples of WT CD4 T cells (green) entering peripheral medullary cords by transmigration through LYVE-1$^+$ endothelium (red, cyan outline) of the capsule-lining sinus floor (see also **Supplementary Video 7**). SHG signal of the LN capsule is shown in blue. Start of *ex vivo* time lapse is 1 h 20 min (**a**) or 35 min (**b**) after intra lymphatic injection of 1.6-2×10$^4$ polyclonal eGFP-expressing WT CD4 T cells. (**c**) Example of a WT CD4 T cell (green) entering peripheral medullary cords by transmigration through LYVE-1$^+$ endothelium (red) after extended migration within the lumen of the peripheral medullary sinus system (see also **Supplementary Video 8**). Time lapse starts 2 h after intra lymphatic injection of 1.6×10$^4$ WT CD4 T cells; scale bars, 10 µm for **a**-**c**. (**d**) Intranodal migration behavior of WT CD4 T cells (tracks in red) within peripheral medullary areas directly after exiting the capsule-lining sinus lumen (white arrowhead). Grey 3D structure illustrates LYVE-1$^+$ lymphatic endothelium and discriminates between peripheral medullary sinus lumen (S) and the parenchyma of peripheral medullary cords (P). Start of *ex vivo* time lapse is 1h after intra lymphatic injection of 1.6×10$^4$ polyclonal WT CD4 T cells, see also **Supplementary Video 9**; scale bar, 20 µm (**e-g**) Statistical analysis of WT CD4 T cell migration behavior within peripheral medullary areas. Migration pathways of 202 individual cells that had left the capsule-lining sinus were carefully analyzed for their distribution between medullary sinus lumen and parenchyma of medullary cords, and for their spatial relationship to the compartment borders (LYVE-1$^+$ lymphatic endothelium). Cell tracks are derived from 3 time lapse recordings (duration 40-60 min) from 3 independent experiments starting 0.5-2 h after intra lymphatic application. Bar graphs depict mean+SD. Scale bar, 20 µm. (**e**) Dwell index (parenchyma vs. sinus lumen, relative to compartment volumes, see Methods for calculation details). A mean dwell index of 2.28 indicates an approximately two-fold preference of intra lymphatically injected WT CD4 T cells for migration within peripheral medullary cords shortly after exiting the capsule-lining sinus. (**f**) Number of transmigration events (i.e. compartment changes by migration

through a LYVE-1$^+$ lymphatic endothelial layer) per cell track. After exit from the capsule-lining sinus, most WT CD4 T cells did not change their compartmental localization during the observation period, and no cell was observed to transmigrate more than three times. Bar graphs show mean relative frequency+SD. (**g**) Localization and direction of transmigration. All WT CD4 T cells analyzed were classified according to the compartment in which they resided at the end of observation: P and S indicate the relative frequency of cell tracks which started as well as ended within peripheral medullary cords, i.e. LN parenchyma (P), or within the lumen of peripheral medullary sinus (S), respectively. ->P and ->S indicate the relative frequency of cell tracks starting within the lumen of peripheral medullary sinus and ending within peripheral medullary cords (-> P) or vice versa (->S).

**Figure 6. CCR7-mediated signals are required for progression of T cells from peripheral medullary areas into the paracortical TCZ.** (**a**) Comparison of the intranodal migration of WT (red, cell tracks in red) and *Ccr7*$^{-/-}$ (green, cell tracks in green) CD4 T cells within peripheral medullary areas. Start of *ex vivo* time lapse (0 min, leftmost panel) is 45 min after intra lymphatic injection of $2.5\times10^4$ total CD4 (1:1), rightmost panel illustrates cell track overlay, SHG signal of the LN capsule is shown in blue. While WT CD4 T cells display an inward migration towards the deeper paracortical TCZ, the random walk-like migration of *Ccr7*$^{-/-}$ CD4 T cells remains confined to peripheral medullary areas (see also **Supplementary Video 10**). (**b**) During migration within peripheral medullary areas, *Ccr7*$^{-/-}$ CD4 T cells display a slightly lower migration velocity compared to WT cells. For average track speed and track straightness, dots represent individual cell tracks, bars indicate median values. Mean displacement plots are calculated using one representative time lapse recording per group. For motility coefficient (MCoeff), dots represent single time lapse recordings of different imaging days, bars indicate mean values, * $P$ <0.05 (unpaired two-tailed Student's $t$ test). Data shown is derived from time lapse recordings of 3 independent experiments starting 45 min to 3.5 h after intra lymphatic

application. (**c**) Immunohistological analysis of CCL21 expression (red) within peripheral medullary areas. Irrespective of the high CCL21 expression on HEV, the intensity of CCL21 staining on parenchymal cells increases towards the LN centre, indicating the existence of an immobilized CCL21 gradient. $CCL21^+$ cells within peripheral medullary cords are directly adjacent to and partially colocalize with LYVE-$1^+$ lymphatic endothelium (blue) of peripheral medullary sinus. White dots outline a B cell follicle devoid of CCL21 signal. Intensity profiles were generated using Fiji. Scale bars, 50 µm for **a**, **c**.

**Figure 7. Transmigration of activated DCs changes the morphology of the afferent side SCS floor and allows direct entry of co-injected T lymphocytes into LN parenchyma.** (**a**) Afferent lymph-derived CD4 T cells (green) alone do not transmigrate through the floor of the afferent side SCS. Start of *ex vivo* time lapse (0 min, left panel) is 30 min after intra lymphatic injection of $2\times10^5$ WT $CD4^+$ cells, SHG signal of the LN capsule is shown in blue. (**b**) $3\times10^3$ TAMRA-labeled WT BMDCs (red) were intra lymphatically injected 40 min prior to application of WT CD4 T cells (green) into the same afferent lymph vessel. Start of *ex vivo* time lapse (0 min, left panel) is 1 h 20 min after intra lymphatic injection of $1.6\times10^4$ WT $CD4^+$ cells, SHG signal of the LN capsule is shown in blue. Overlay of WT CD4 T cell tracks (green) is shown in the right panel; scale bars, 50 µm for **a**,**b**. (**c, d**) Cellular composition and morphology of the SCS remains unchanged after intra lymphatic injection of 6 µm beads or WT CD4 T cells alone (both shown in green). The SCS floor of the afferent side of the popLN is composed a thin layer of LYVE-$1^+$ lymphatic endothelial cells (red) as well as numerous $CD169^+$ SCS-lining macrophages (blue) that extend into the SCS lumen (see insets). (**e**) Activated DCs ($eGFP^+$ WT BMDCs, green) induce profound changes of the SCS floor morphology during transmigration. SCS-lining $CD169^+$ macrophages (blue) appear elongated while the LYVE-1-staining (red) is largely diminished (left inset). This effect is locally restricted to parts of the SCS with high concentrations of intra lymphatically injected DCs (compare with the steady-state SCS floor morphology of left inset); scale bars, 100 µm for **c**-**e**.

# Methods

**Animals.** Mice were bred at the central animal facility of Hannover Medical School under specific pathogen-free conditions or purchased from Charles River. Mouse strains used: C57BL/6, B6.129P2(C)-Ccr7$^{tm1Rfor}$/J[1], backcrossed on C57BL/6 for >15 generations (designated *Ccr7*$^{-/-}$), B6.C-H2$^{bm1}$ (H2-K$^{bm1}$), C57BL/6-Tg(Tcra Tcrb)1100MjbJ Ly5.1 (ref.[35]), specifically recognizing the ovalbumin-derived SIINFEKL-peptide presented in the context of MHC class I (designated OT-I Ly5.1), B6.CD11c-eYFP[34], B6.beta-act-eGFP[36] and B6.beta-act-eGFP×*Ccr7*$^{-/-}$. All animal experiments have been approved by the institutional review board and the *Niedersächsische Landesamt für Verbraucherschutz und Lebensmittelsicherheit;* LAVES.

**Antibodies and reagents.** Antibodies and conjugates used: Anti-MHCII-PE (clone M5-114.15.2; BioLegend), anti-CD11c-PE-Cy7 (N418), anti-CD86-APC (GL1), anti-CD45.1-PE-Cy7 (A20), anti-CD45.2-PerCP-Cy5.5 (104), anti-LYVE-1-eFluor660 (ALY7; all from eBioscience), anti-LYVE-1 (Acris), mouse-anti-rabbit-Cy5, mouse-anti-rabbit-Cy3 (both from Jackson), anti-CCL21 (R&D), anti-TCR Vα2-PE (B20.1), anti-TCR Vß5-bio (MR9-4; both from Pharmingen), anti-CD169-AlexaFluor647 (MOMA-1; AbD Serotec), Streptavidin-Cy5 (Caltag). Anti-IgD (HB250) and anti-CD8α (53-6.7) antibodies were provided by E. Kremmer (Helmhotz Zentrum München, Germany). Cy5 conjugation was performed as recommended by the manufacturer (GE Healthcare). Further reagents: 6 µm yellow-green fluorescent polystyrene latex microspheres (Polysciences), paraformaldehyde-fixable FITC-conjugated 500 kDa Dextran (Molecular Probes), DAPI (Sigma-Aldrich).

**Generation of bone marrow-derived DCs.** DCs were generated *in vitro* from BM precursors as previously described [2] and treated with 1 µg/ml LPS (Sigma-Aldrich) during the last 24 h of culture. In all cases, DC differentiation and maturation status were assessed by analyzing expression of CD11c, MHCII and CD86 prior to intra lymphatic injection.

**Intralymphatic injection.** Mice were anesthetized by intraperitoneal injection of 600 mg/kg ketamine (Ketamin, Gräub) and 1 mg/kg medetomidine (Domitor, Pfizer). After shaving and depilating one calf, a longitudinal skin incision of ~1 cm was made on the dorsal side of the lower hind leg. A borosilicate glass capillary (OD 1.5 mm, ID 1.17 mm, Harvard Apparatus), pulled manually and grinded using an EG-44 micropipette grinder (Narishige), was filled with 5 µl cell suspension (in PBS) using a PLI-100 microinjector (Harvard Apparatus). A micromanipulator (MN-151, Narishige) was used to stabilize the capillary during the injection. Pressure of approximately 5 kPa in 90 sec long pulses was used to deliver the cells. The number of cell delivered in three pulses was determined in preliminary experiments and the concentration of cells aspirated was calculated accordingly to yield the number of delivered cells shown in the individual experiments. At all times during surgery, exposed tissue was kept moist with sterile PBS. The incision was closed with tissue adhesive (Nexabond) at the end of surgery. In some experiments, cells were labeled with 10 µM 5-(and-6-)-TAMRA-SE or 25 µM DDAO-SE (Invitrogen) for 15 min at 37°C prior to intra lymphatic application. If co-injected with exogenously labeled cells, eGFP-expressing cells were subjected to the same staining procedure without applying the dye.

**DCs retrieval.** Wild-type and *Ccr7*$^{-/-}$ BM-derived DCs were labeled with TAMRA or DDAO (and vice versa) as described above and mixed at a ratio of 1:1. At 2h after intra lymphatic delivery of 2.5x10$^5$ DCs, LN were mechanically disrupted using fine forceps and digested with 100 µg/ml Blendzyme2 and 0.3 mg/ml DNase (Roche) in RPMI 1640 (Invitrogen) for 30 min at 37 °C shaking at 100 rpm. For identification of DCs, FACS data was pre-gated on singlet events according to the forward scatter width/height-profile. The retrieval ratio was corrected to account for the exact input mixture composition.

**Skin DCs preparation.** Mice were sacrificed and ears of CD11c-YFP mice were briefly rinsed with ethanol and air-dried. Subsequently, ears were split in halves using fine forceps, and the dorsal halves were incubated for 3 days floating on DC medium with the dermal side facing down as described elsewhere[2]. During the last 24h of incubation and equally to BMDCs treatment, 1 µg/ml LPS (Sigma-Aldrich) was added to the medium. DCs that had emigrated into the culture medium showed a mature phenotype als determined by flow cytometry. Cells were harvested by centrifugation and used for i.l injection.

**LN shutdown.** $0.5\times10^3$ or $1\times10^5$ BM-derived LPS-matured DCs (WT or *Ccr7*$^{-/-}$) were applied by intra lymphatic or subcutaneous injection. 72h later, total cell counts of the draining popLN were determined.

**Immunohistology.** After rehydration and preincubation with 10% rat serum, 8 µm-thick paraformaldehyde (2% + 30% sucrose)-fixed LN-cryosections were stained with conjugated antibodies and DAPI. High resolution composite images were acquired using a Zeiss Axiovert 200 M microscope.

**3D LN-reconstruction.** Immunohistological staining and imaging was performed with all cryosections of a single LN as described above. Composite images were imported as TIFF-files into the TrackEM function of the image analysis software Fiji (**F**iji **i**s **j**ust **I**mageJ, open-source: http://pacific.mpi-cbg.de/wiki/index.php/Fiji). After manual alignment and cropping, TIFF-stacks were exported to Imaris 7.0 (Bitplane) for further visualization. Single sections containing substantial artefacts were replaced by a directly adjacent section.

**T cell proliferation.** At day -1, lymphocytes were isolated from peripheral LN (pLN) and spleen of OT-I Ly5.1 mice and labeled with CFSE as described previously[37]. 1.5 x $10^7$ cells were injected i.v. into each C57BL/6 bm1 recipient. At day 0, BMDCs were loaded with SIINFEKL-peptide (5 µg/ml) during the last hour of *in vitro* culture, and $5\times10^3$ BMDCs per recipient were transferred by intra

lymphatic injection. 65 h later, mice were sacrificed, and various LN were analyzed by flow cytometry. Gating on $CD8^+$, Ly $5.1^+$, $V\alpha2^+$ and $V\beta5^+$, the CFSE profile of OT-I ovalbumin T cells was analyzed using the automated proliferation function of FlowJo (Treestar). The number of proliferation cycles was adjusted to obtain an equation with the smallest root mean square.

**$CD4^+$ T cell preparation.** Lymphocytes were isolated from pooled peripheral LN and spleens of 6-8 week old wild type or *Ccr7*$^{-/-}$ donor mice, and $CD4^+$ T cells were enriched to a purity of 90-95% by AutoMACS using the MACS $CD4^+$ Negative Isolation Kit (Miltenyi Biotec).

**Two-photon microscopy.** At various points of time after intra lymphatic injection, mice were sacrificed, and the explanted popLN was mounted in a custom-built incubation chamber. Two-photon microscopy using a TriM Scope setup (LaVision Biotec) was performed as described before [17, 38], tuning to 920 nm for best visualization of eGFP and eYFP. For each genotype, 1500-7500 DCs or $1.25\text{-}2\times10^4$ CD4 T cells were injected intralymphatically for subsequent two-photon imaging. Lymphatic endothelium of the popLN was labeled by intra lymphatic injecting 5 µg anti-LYVE-1 Ab labeled with eFluor660 30 min prior to the intra lymphatic application of cells. Antibody staining was visualized by fluorochrome-excitation with an OPO device (APE) tuned to 1100 nm. Imaging experiments were also performed using an *in vivo* microscopy setup described before[14]. Imaris 7 (Bitplane) was used for semi-automated cell tracking applying the following criteria. Cells not being inside the imaging volume with their entire cell body as well as immotile cells underlying the capsule were excluded from track analysis. Similarly, DCs that did not show any dendrite movement were not considered. Minimal track duration was set to 3 min for DCs and 1 min for T cells to be included in quantitative track analysis. Primary data analysis was done in Imaris, mean displacement and motility coefficient values were calculated using VBA macros in Excel (Microsoft). The dwell index characterizing CD4 T cell migration was calculated as

$$\frac{\sum \text{duration of all track parts in compartment A} \,/\, \sum \text{duration of all track parts in compartment B}}{\text{volume of compartment A} \,/\, \text{volume of compartment B}}$$

and equals 1 if cells are evenly distributed within both compartments. The isosurface function of Imaris was used to visualize LYVE-1$^+$ sinus structures and to determine compartment volumes. Since our initial experiments revealed no obvious differences between the two setups regarding cellular dynamics and migration behavior of DCs (as quantified by various motility parameters such as velocity and directionality), the majority of experiments were performed using popLN explants. Unfortunately, the medullary regions of the popLN are not accessible to *in vivo* imaging due to their anatomic localization in the very depth of the popliteal fossa. Therefore, we could only address on explanted LN but not by *in vivo* imaging the migration behavior of T cells arriving via afferent lymphatic in medullary regions of the popLN.

**CCL21 intensity profile.** The Fiji software package was used to automatically calculate mean pixel intensities of the fluorescence channels representing CCL21 and LYVE-1 relative to the distance from the LN capsule.

**Statistical analysis.** Statistical analysis was performed with Prism4 (GraphPad). The unpaired two-tailed Student's *t* test was used to test for statistical significance.

## References

37. Worbs, T. *et al.* Oral tolerance originates in the intestinal immune system and relies on antigen carriage by dendritic cells. *J Exp Med* **203**, 519-527 (2006).

38. Halle, S. *et al.* Induced bronchus-associated lymphoid tissue serves as a general priming site for T cells and is maintained by dendritic cells. *J Exp Med* **206**, 2593-2601 (2009).

## References

1. Forster, R. *et al.* CCR7 coordinates the primary immune response by establishing functional microenvironments in secondary lymphoid organs. *Cell* **99**, 23-33 (1999).

2. Ohl, L. *et al.* CCR7 governs skin dendritic cell migration under inflammatory and steady-state conditions. *Immunity* **21**, 279-288 (2004).

3. Ouwehand, K. *et al.* CXCL12 is essential for migration of activated Langerhans cells from epidermis to dermis. *Eur J Immunol* **38**, 3050-3059 (2008).

4. Saeki, H., Moore, A.M., Brown, M.J. & Hwang, S.T. Cutting edge: secondary lymphoid-tissue chemokine (SLC) and CC chemokine receptor 7 (CCR7) participate in the emigration pathway of mature dendritic cells from the skin to regional lymph nodes. *J Immunol* **162**, 2472-2475 (1999).

5. Baluk, P. *et al.* Functionally specialized junctions between endothelial cells of lymphatic vessels. *J Exp Med* **204**, 2349-2362 (2007).

6. Lammermann, T. *et al.* Rapid leukocyte migration by integrin-independent flowing and squeezing. *Nature* **453**, 51-55 (2008).

7. Pflicke, H. & Sixt, M. Preformed portals facilitate dendritic cell entry into afferent lymphatic vessels. *J Exp Med* **206**, 2925-2935 (2009).

8. Bromley, S.K., Thomas, S.Y. & Luster, A.D. Chemokine receptor CCR7 guides T cell exit from peripheral tissues and entry into afferent lymphatics. *Nat Immunol* **6**, 895-901 (2005).

9. Debes, G.F. *et al.* Chemokine receptor CCR7 required for T lymphocyte exit from peripheral tissues. *Nat Immunol* **6**, 889-894 (2005).

10. Luther, S.A., Tang, H.L., Hyman, P.L., Farr, A.G. & Cyster, J.G. Coexpression of the chemokines ELC and SLC by T zone stromal cells and deletion of the ELC gene in the plt/plt mouse. *Proc Natl Acad Sci U S A* **97**, 12694-12699 (2000).

11. Link, A. *et al.* Fibroblastic reticular cells in lymph nodes regulate the homeostasis of naive T cells. *Nat Immunol* **8**, 1255-1265 (2007).

12. Tomei, A.A., Siegert, S., Britschgi, M.R., Luther, S.A. & Swartz, M.A. Fluid flow regulates stromal cell organization and CCL21 expression in a tissue-engineered lymph node microenvironment. *J Immunol* **183**, 4273-4283 (2009).

13. Stein, J.V. *et al.* The CC chemokine thymus-derived chemotactic agent 4 (TCA-4, secondary lymphoid tissue chemokine, 6Ckine, exodus-2) triggers lymphocyte function-associated antigen 1-mediated arrest of rolling T lymphocytes in peripheral lymph node high endothelial venules. *J Exp Med* **191**, 61-76 (2000).

14. Worbs, T., Mempel, T.R., Bolter, J., von Andrian, U.H. & Forster, R. CCR7 ligands stimulate the intranodal motility of T lymphocytes in vivo. *J Exp Med* **204**, 489-495 (2007).

15. Gunn, M.D. *et al.* Mice lacking expression of secondary lymphoid organ chemokine have defects in lymphocyte homing and dendritic cell localization. *J Exp Med* **189**, 451-460 (1999).

16. Harrell, M.I., Iritani, B.M. & Ruddell, A. Lymph node mapping in the mouse. *J Immunol Methods* **332**, 170-174 (2008).

17. Bakocevic, N., Worbs, T., Davalos-Misslitz, A. & Forster, R. T cell-dendritic cell interaction dynamics during the induction of respiratory tolerance and immunity. *J Immunol* **184**, 1317-1327 (2010).

18. Yanagawa, Y. & Onoe, K. CCL19 induces rapid dendritic extension of murine dendritic cells. *Blood* **100**, 1948-1956 (2002).

19. MartIn-Fontecha, A. *et al.* Regulation of dendritic cell migration to the draining lymph node: impact on T lymphocyte traffic and priming. *J Exp Med* **198**, 615-621 (2003).

20. Byrne, S.N., Halliday, G.M., Johnston, L.J. & King, N.J. Interleukin-1beta but not tumor necrosis factor is involved in West Nile virus-induced Langerhans cell migration from the skin in C57BL/6 mice. *J Invest Dermatol* **117**, 702-709 (2001).

21. Cahill, R., Hay, J.B., Frost, H. & Trnka, Z. Changes in lymphocyte circulation after administration of antigen. *Haematologia (Budap)* **8**, 321-334 (1974).

22. Hintzen, G. *et al.* Induction of tolerance to innocuous inhaled antigen relies on a CCR7-dependent dendritic cell-mediated antigen transport to the bronchial lymph node. *J Immunol* **177**, 7346-7354 (2006).

23. Schumann, K. *et al.* Immobilized chemokine fields and soluble chemokine gradients cooperatively shape migration patterns of dendritic cells. *Immunity* **32**, 703-713 (2010).

24. Bajenoff, M. *et al.* Stromal cell networks regulate lymphocyte entry, migration, and territoriality in lymph nodes. *Immunity* **25**, 989-1001 (2006).

25. Mempel, T.R., Junt, T. & von Andrian, U.H. Rulers over randomness: stroma cells guide lymphocyte migration in lymph nodes. *Immunity* **25**, 867-869 (2006).

26. Pham, T.H., Okada, T., Matloubian, M., Lo, C.G. & Cyster, J.G. S1P1 receptor signaling overrides retention mediated by G alpha i-coupled receptors to promote T cell egress. *Immunity* **28**, 122-133 (2008).

27. Grigorova, I.L. *et al.* Cortical sinus probing, S1P1-dependent entry and flow-based capture of egressing T cells. *Nat Immunol* **10**, 58-65 (2009).

28. Grigorova, I.L., Panteleev, M. & Cyster, J.G. Lymph node cortical sinus organization and relationship to lymphocyte egress dynamics and antigen exposure. *Proc Natl Acad Sci U S A* **107**, 20447-20452 (2010).

29. Schwab, S.R. & Cyster, J.G. Finding a way out: lymphocyte egress from lymphoid organs. *Nat Immunol* **8**, 1295-1301 (2007).

30. Spiegel, S. & Milstien, S. The outs and the ins of sphingosine-1-phosphate in immunity. *Nat Rev Immunol* **epub ahead of print** (2011).

31. Lo, C.G., Xu, Y., Proia, R.L. & Cyster, J.G. Cyclical modulation of sphingosine-1-phosphate receptor 1 surface expression during lymphocyte recirculation and relationship to lymphoid organ transit. *J Exp Med* **201**, 291-301 (2005).

32. Matloubian, M. *et al.* Lymphocyte egress from thymus and peripheral lymphoid organs is dependent on S1P receptor 1. *Nature* **427**, 355-360 (2004).

33. Kissenpfennig, A. *et al.* Dynamics and function of Langerhans cells in vivo: dermal dendritic cells colonize lymph node areas distinct from slower migrating Langerhans cells. *Immunity* **22**, 643-654 (2005).

34. Lindquist, R.L. *et al.* Visualizing dendritic cell networks in vivo. *Nat Immunol* **5**, 1243-1250 (2004).

35. Nikolic-Zugic, J. & Bevan, M.J. Role of self-peptides in positively selecting the T-cell repertoire. *Nature* **344**, 65-67 (1990).

36. Okabe, M., Ikawa, M., Kominami, K., Nakanishi, T. & Nishimune, Y. 'Green mice' as a source of ubiquitous green cells. *FEBS Lett* **407**, 313-319 (1997).

# Fig.1

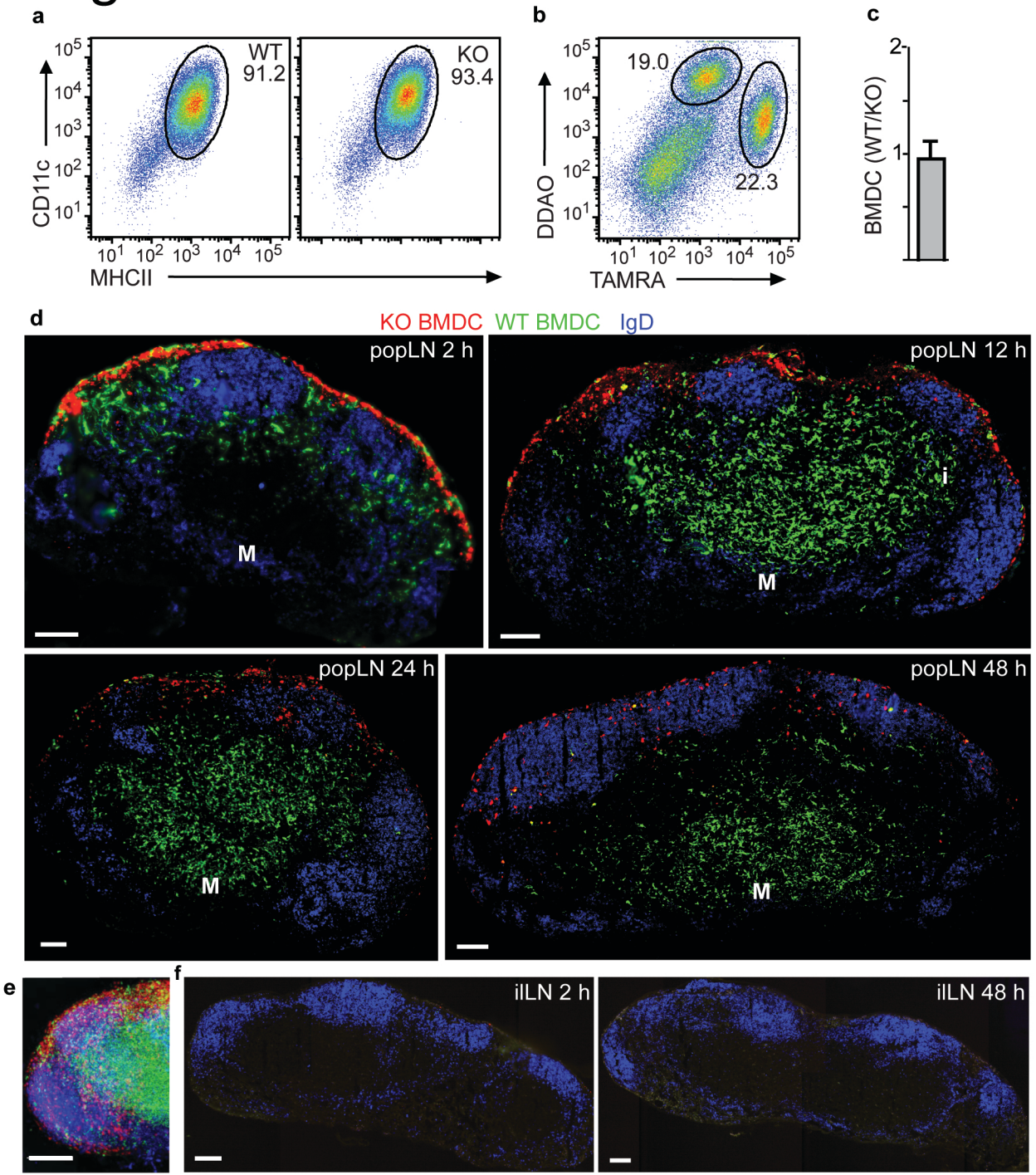
a
WT
91.2
KO
93.4
CD11c
MHCII
b
19.0
22.3
DDAO
TAMRA
c
BMDC (WT/KO)
d
KO BMDC WT BMDC IgD
popLN 2 h
popLN 12 h
popLN 24 h
popLN 48 h
M
i
e
f
iILN 2 h
iILN 48 h

# Fig. 2

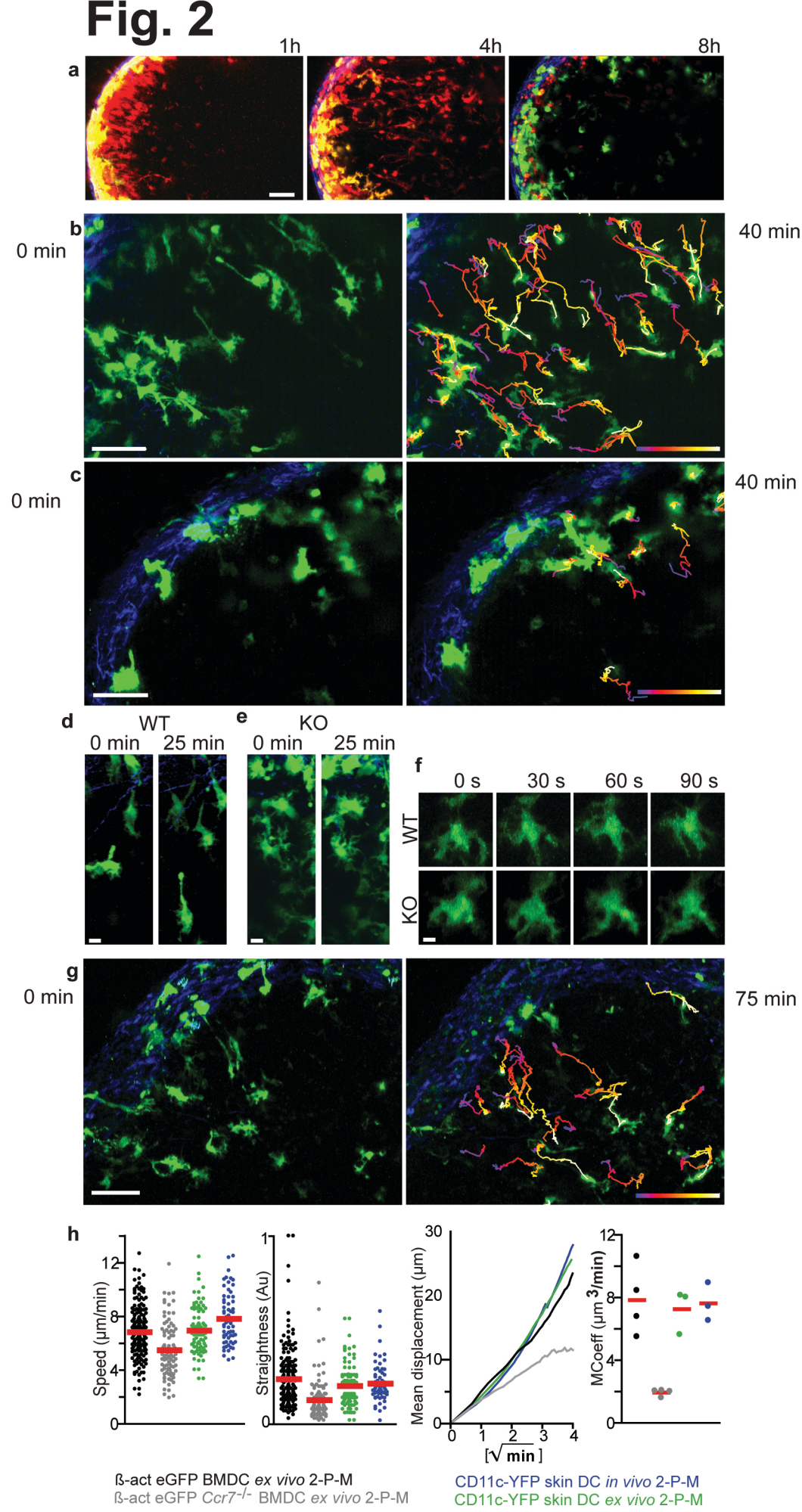
a
1h
4h
8h
b
0 min
40 min
c
0 min
40 min
d
WT
0 min
25 min
e
KO
0 min
25 min
f
0 s
30 s
60 s
90 s
WT
KO
g
0 min
75 min
h
Speed (µm/min)
Straightness (Au)
Mean displacement (µm)
[√ min ]
MCoeff (µm 3/min)
ß-act eGFP BMDC ex vivo 2-P-M
ß-act eGFP Ccr7-/- BMDC ex vivo 2-P-M
CD11c-YFP skin DC in vivo 2-P-M
CD11c-YFP skin DC ex vivo 2-P-M

# Fig. 3

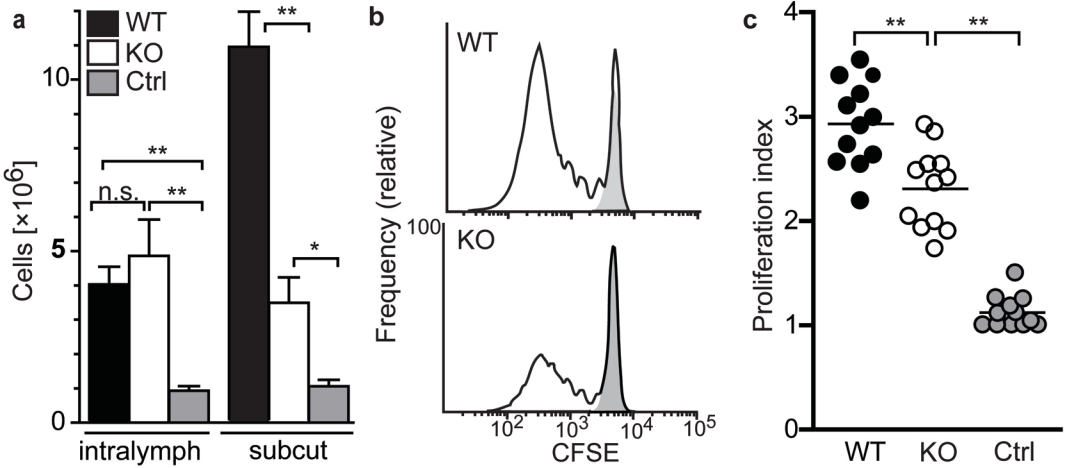
a
WT
KO
Ctrl
Cells [×10^6]
10
5
0
**
n.s.
**
**
*
intralymph
subcut
b
WT
KO
Frequency (relative)
100
10^2
10^3
10^4
10^5
CFSE
c
Proliferation index
4
3
2
1
0
**
**
WT
KO
Ctrl

Fig. 4

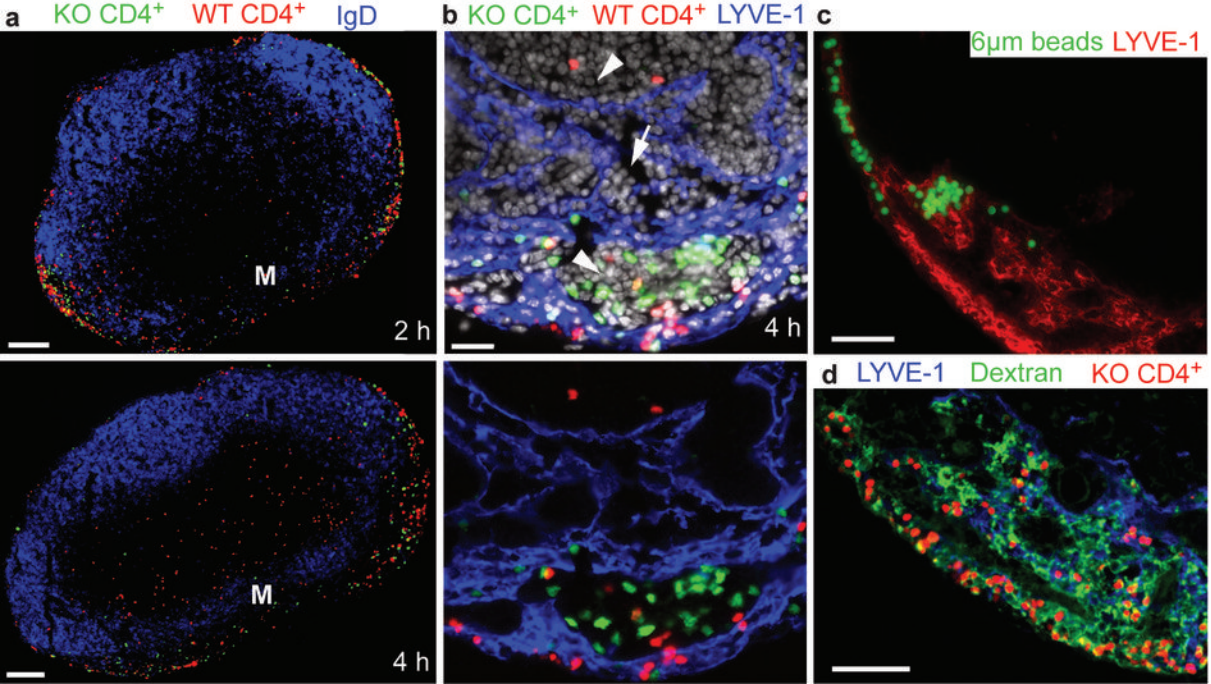
a KO CD4+ WT CD4+ IgD
M
2 h
M
4 h
b KO CD4+ WT CD4+ LYVE-1
4 h
c
6μm beads LYVE-1
d LYVE-1 Dextran KO CD4+

Fig. 5

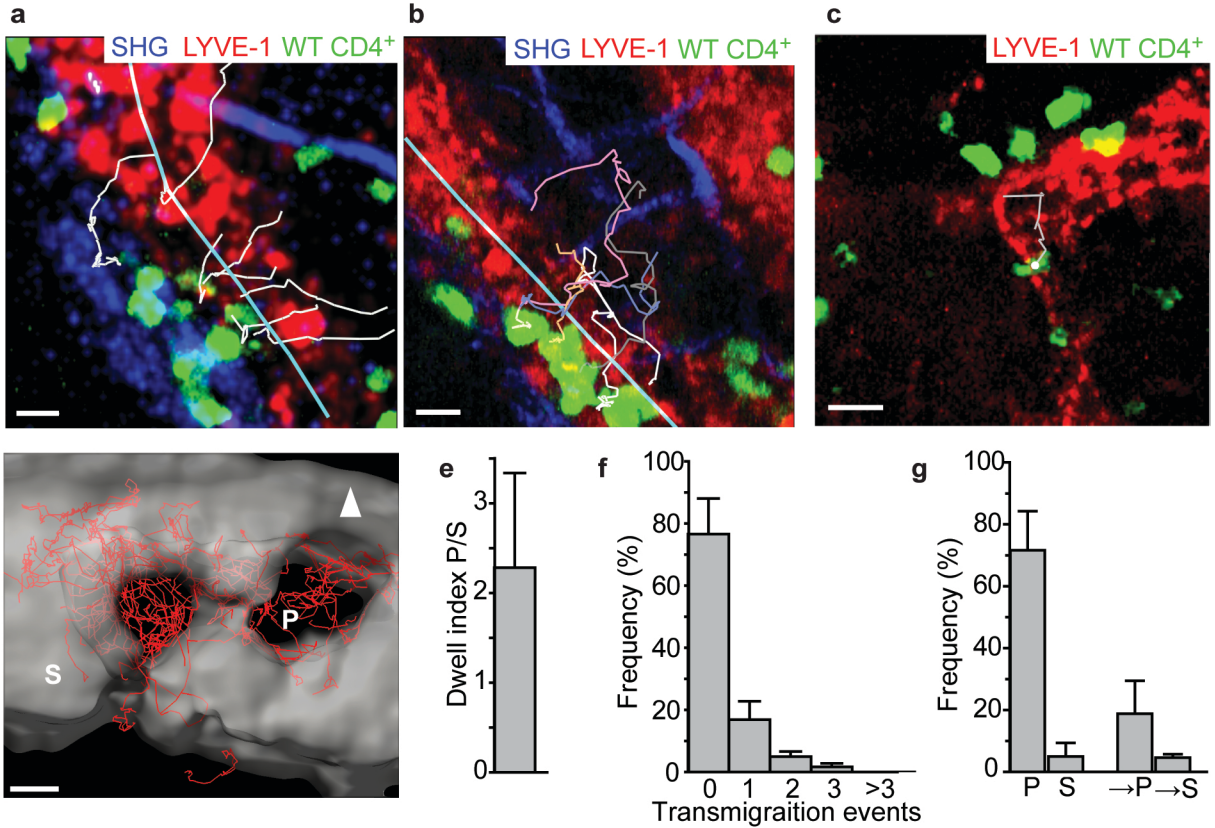
a
SHG LYVE-1 WT CD4+
b
SHG LYVE-1 WT CD4+
c
LYVE-1 WT CD4+
d
P
S
e
Dwell index P/S
0
1
2
3
f
Frequency (%)
0
20
40
60
80
100
0 1 2 3 >3
Transmigraition events
g
Frequency (%)
0
20
40
60
80
100
P S →P→S

Fig. 6

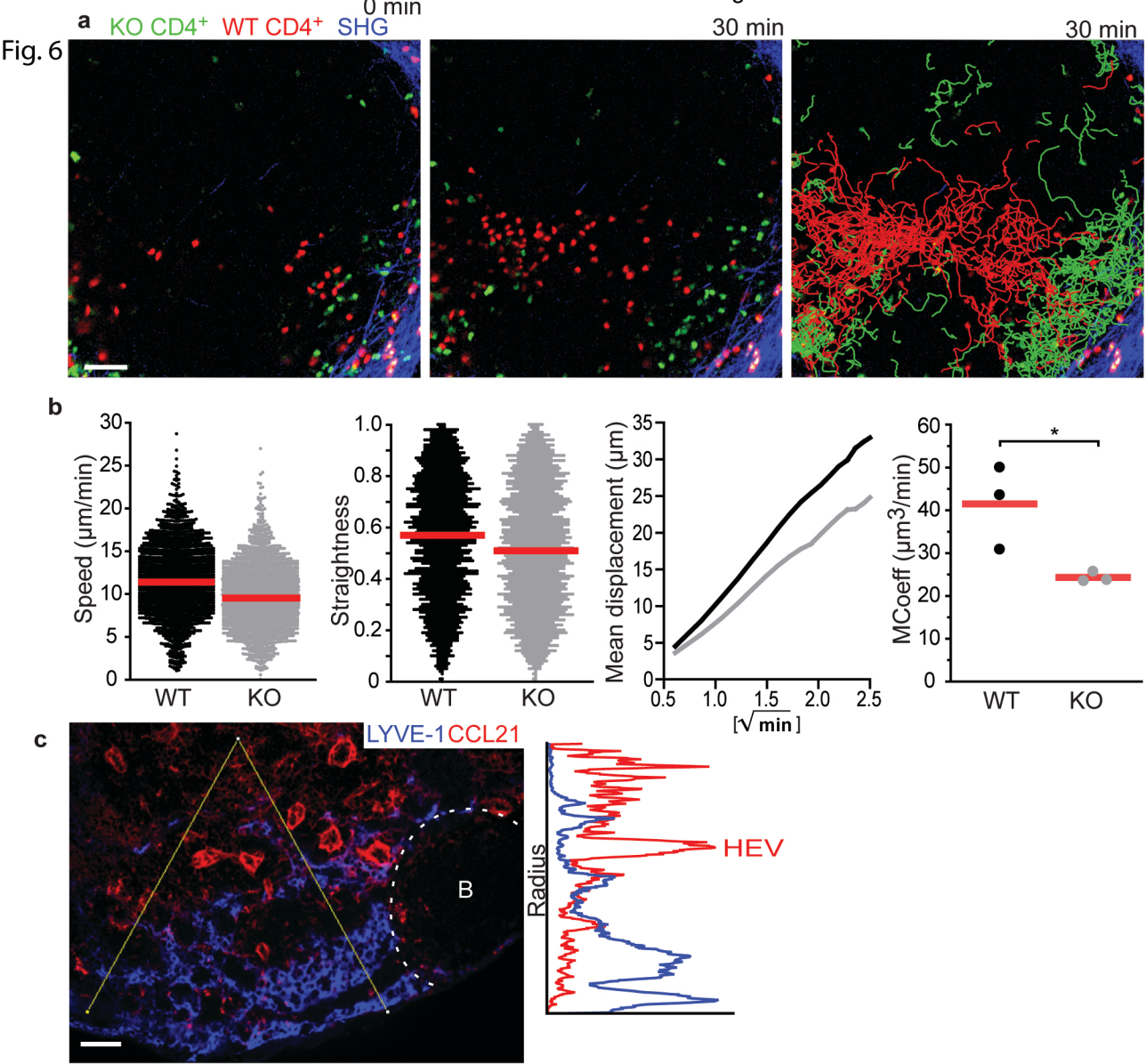
a
KO CD4+ WT CD4+ SHG
0 min
30 min
30 min
b
Speed (μm/min)
WT
KO
Straightness
WT
KO
Mean displacement (μm)
[√min]
MCoeff (μm3/min)
*
WT
KO
c
LYVE-1CCL21
B
Radius
HEV

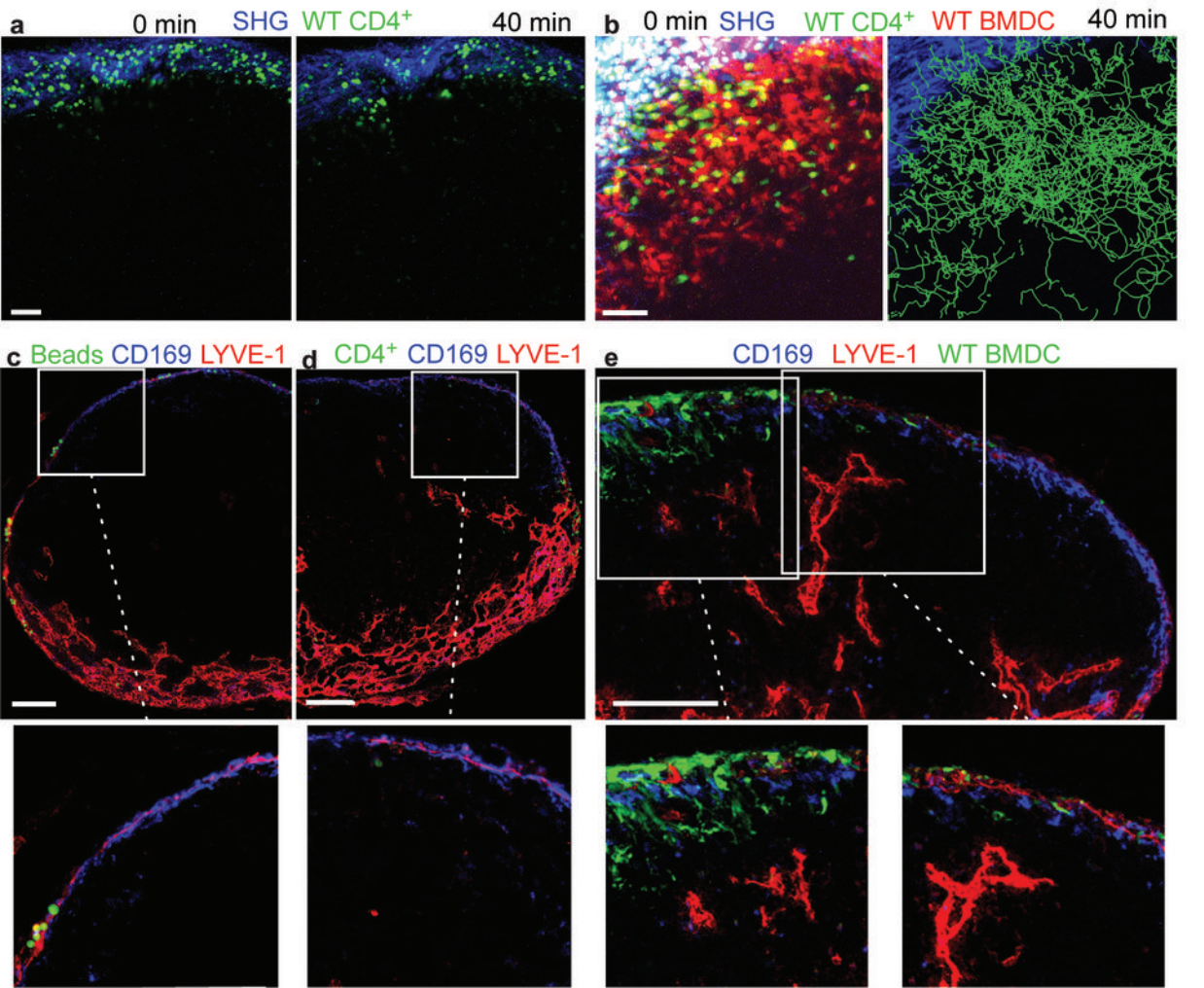
a
0 min
SHG
WT CD4+
40 min
b
0 min
SHG
WT CD4+
WT BMDC
40 min
c
Beads
CD169
LYVE-1
d
CD4+
CD169
LYVE-1
e
CD169
LYVE-1
WT BMDC